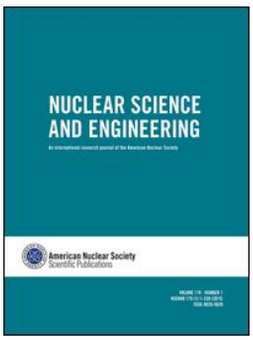

Nuclear Science and Engineering

ISSN: 0029-5639 (Print) 1943-748X (Online) Journal homepage: http://www.tandfonline.com/loi/unse20

Prediction of the Prompt Neutron Multiplicity Distribution $\nu(A)$ for $^{235}U(n,f)$ and $^{239}Pu(n,f)$ in the Incident Energy Range of Multichance Fission

Anabella Tudora, Franz-Josef Hambsch & Viorel Tobosaru

To cite this article: Anabella Tudora, Franz-Josef Hambsch & Viorel Tobosaru (2018): Prediction of the Prompt Neutron Multiplicity Distribution $\nu(A)$ for $^{235}U(n,f)$ and $^{239}Pu(n,f)$ in the Incident Energy Range of Multichance Fission, Nuclear Science and Engineering, DOI: 10.1080/00295639.2018.1497394

To link to this article: https://doi.org/10.1080/00295639.2018.1497394

Published online: 17 Aug 2018.

NUCLEAR SCIENCE AND ENGINEERING

DOI: https://doi.org/10.1080/00295639.2018.1497394

Prediction of the Prompt Neutron Multiplicity Distribution $\nu(A)$ for ^{235}U(n,f) and ^{239}Pu(n,f) in the Incident Energy Range of Multichance Fission

Anabella Tudora,[a]* Franz-Josef Hambsch,[b] and Viorel Tobosaru[a]

[a]*University of Bucharest, Faculty of Physics, Bucharest-Magurele, Str. Atomistilor 405, RO-77125, POB MG-11, Romania*
[b]*European Commission, Joint Research Centre, Directorate G, Unit G2, Retieseweg 111, B-2440, Geel, Belgium*

Received February 8, 2018
Accepted for Publication July 3, 2018

Abstract — *Measurements of fission fragment data at incident energies (En) up to several tens of MeV require prompt neutron multiplicity distribution ν(A) to determine the preneutron fragment properties. Those ν(A) data are not readily experimentally available. Consequently, model predictions of ν(A) at En where multichance fission occurs are needed. The Point-by-Point model of prompt emission provides the individual ν(A) of compound nuclei of the main and secondary nucleus chains that are undergoing fission at any En. Total ν(A) calculations for n + ^{235}U and n + ^{239}Pu are presented together with systematic behaviors of individual ν(A) with increasing energy.*

Keywords — *Prompt emission in fission, prompt fission neutron distributions, average number of prompt neutrons, fission fragment distributions.*

Note — *Some figures may be in color only in the electronic version.*

I. INTRODUCTION

The need for accurate nuclear fission data for new applications (e.g., advanced nuclear systems, incineration of nuclear waste, production of isotopes, etc.) and for better knowledge of the fission process implies the study of neutron-induced fission of actinides at intermediate and high energies.

The fission fragment mass distribution $Y(A)$ is one of the most important characteristics of prompt fission. In the last years nuclear modelings have made large progress, but a pure theoretical description of $Y(A)$ is not yet achieved. For this reason the experimental data of preneutron fragment mass and kinetic energy distributions $Y(A,TKE)$ are preferred in prompt emission calculations. A great part of measurements regarding fragment distributions was focused on actinide fissioning with thermal neutrons and eventually with neutron energies below the threshold of second-chance fission. Recently, experiments concerning postneutron fragment distributions of neutron-induced fission of ^{238}U, ^{235}U, and ^{239}Pu with energies from hundreds of keV up to several tens of MeV were performed at the Los Alamos Neutron Science Center – Weapons Neutron Research (LANSCE-WNR). The detector used was a Frisch-gridded ionization chamber, and the double-energy analysis technique was employed to calculate the preneutron and postneutron emission data.[1–3]

To recover the preneutron fragment masses and distributions from the experimental postneutron fragment data, prompt neutron multiplicity distributions $\nu(A)$ are needed. The experimental $\nu(A)$ data are very scarce, being measured for only a few actinides and only at incident neutron energies (En) below the second-chance fission threshold, i.e., from thermal En up to about 5 MeV. The $\nu(A)$ data at thermal En are the most numerous. Experimental $\nu(A)$ data at En above 5 to 6 MeV (where multiple fission chances are involved) are

*E-mail: anabellatudora@hotmail.com

completely missing. This lack of data can be compensated only by model predictions of $\nu(A)$.

The Point-by-Point (PbP) model of prompt emission has answered the need of $\nu(A)$ at En where multichance fission occurs by the $\nu(A)$ prediction for the neutron-induced fission of ^{238}U up to En = 80 MeV (Refs. 4 and 5).

The prediction of $\nu(A)$ for the fast neutron–induced fission of other two major actinides, ^{235}U and ^{239}Pu, based on the modeling and the indirect validation procedure described in Ref. 4, is very important for at least two points of view:

1. the envisage of a systematic behavior of individual $\nu(A)$ distributions with increasing excitation energy of the fissioning nucleus, which contributes to a better knowledge of the prompt neutron emission at high energies
2. a practical purpose, i.e., the need of $\nu(A)$ (at En up to several tens of MeV) in the recovering of pre-neutron fragment distributions from the measured postneutron fragment data.

The PbP model provides the individual $\nu(A)$ of all compound nuclei undergoing fission at each En. The fission probabilities of these compound nuclei are taken as fission cross-section ratios (RFs) of the ENDF/B-VIII evaluation.[6]

The only experimental prompt neutron data existing in a large amount and covering a large En range (from thermal up to more than 20 MeV) are referring to the total average number of prompt neutrons $<\nu>_{tot}$ for both reactions n + ^{235}U and n + ^{239}Pu. These experimental data make an indirect validation of $\nu(A)$ possible at En above the threshold of second-chance fission.

To our knowledge, only PbP results of $\nu(A)$ at En where multichance fission occurs were reported (published).[4,5] Other computer codes (e.g., CGMF, FREYA) include the possibility of prompt emission calculation at En up to 20 MeV. But, up to now, $\nu(A)$ results of these codes at En above the threshold of the second-chance fission have not been reported. The GEF code (Ref. 7 and references therein) also provides $\nu(A)$ at En where multichance fission occurs. This code is very popular especially for experimentalists because it is freely accessible and has a very simple input (requiring only the mass and charge of the fissioning nucleus and the type of fission). The $\nu(A)$ results of GEF were already used in a first preliminary treatment of postneutron data measured at LANSCE-WNR reported in Refs. 1, 2, and 3. For these reasons the PbP results of this paper are compared with the ones of the GEF code.

II. BASIC FEATURES OF THE MODELING

At each En, PbP model calculations are performed for each compound nucleus undergoing fission (which is formed at the respective En) at its average excitation energy. The average excitation energies of the fissioning nuclei acting at a given En are obtained recursively on the basis of the average excitation energy of the precursor, the average energy of the emitted particle, and its separation energy from the precursor.

If the En is less than 25 to 30 MeV, only the fissioning nuclei of the main nucleus chain (resulting from neutron emission from the precursor of this chain) are formed. Their average excitation energies at a given En are calculated recursively as

$$Ex_1^{(1)} = En + Bn_1^{(1)}$$
$$\langle Ex\rangle_i^{(1)} = \langle Ex\rangle_{i-1}^{(1)} - Bn_{i-1}^{(1)} - \langle \varepsilon_n\rangle_{i-1}^{(1)} \quad i = 2, \ldots, N^{(1)} \ , \ (1)$$

where

i = compound nucleus undergoing fission (or the fission chance)

$N^{(1)}$ = number of compound nuclei of the main chain formed at a given En

$\langle Ex\rangle^{(1)}$ = average excitation energies of these nuclei

$Bn^{(1)}$ = neutron binding energies in these compound nuclei

$\langle \varepsilon_n\rangle^{(1)}$ = average center-of-mass energies of the neutrons emitted before fission.

At En above 30 MeV, the charged particle emission occurs, and the fission of compound nuclei of the secondary chains formed by different paths must be taken into account. The recursive formulas giving the average excitation energies of the fissioning nuclei formed by six paths can be found in Ref. 8, i.e., the following ways/paths:

1. "proton" emission from the nuclei of the main chain, leading to the formation of the first secondary nucleus chain), usually denoted as "p"
2. "neutron via proton" (denoted as "pn") consisting of the successive neutron evaporation from the precursor of the first secondary chain
3. "deuteron" emission (denoted as "d") from the nuclei of the main chain, leading to nuclei of the first secondary chain, too

4. "alpha" emission (denoted as "α") from the nuclei of the main chain, leading to the formation of the second secondary nucleus chain
5. "neutron via alpha" (denoted as "nα") consisting of the successive neutron emission from the precursor of the second secondary nucleus chain formed by alpha emission.

The fission probabilities of each compound nucleus formed by the ways mentioned above are expressed by the so-called total and partial *RF* (Ref. 8). At *En* up to about 50 to 60 MeV, only the secondary compound nuclei formed by the "proton" and "neutron via proton" ways are taken into account, the contribution of other ways (e.g., "alpha", "neutron via alpha," etc.) becoming significant above 60 MeV (see Ref. 8 for more details).

The average excitation energies of the compound nuclei formed by the "proton" and "neutron via proton" ways are given by the following recursive relations[4,8]:

$$\langle Ex\rangle_i^{(p)} = \langle Ex\rangle_i^{(1)} - Sp_i^{(1)} - \langle \varepsilon_p \rangle_i \quad i = 1, \ldots, N^{(2)} \qquad (2)$$

and

$$\langle Ex\rangle_i^{(pn)} = \langle Ex\rangle_{i-1}^{(pn)} - Sn_{i-1}^{(2)} - \langle \varepsilon_n \rangle_{i-1}^{(2)} \quad i = 2, \ldots, N^{(2)}$$
$$\langle Ex\rangle_1^{(pn)} = \langle Ex\rangle_1^{(p)} \ , \qquad (3)$$

where

$N^{(2)}$ = number of compound nuclei of the first secondary chain [denoted as (2)]

$Sp^{(1)}$ = proton separation energies from the nuclei of the main chain (1)

$Sn^{(2)}$ = neutron separation energies from the nuclei of the secondary chain (2)

$\langle \varepsilon_p \rangle$, $\langle \varepsilon_n \rangle^{(2)}$ = average center-of-mass energies of the evaporated proton and neutron before fission, respectively.

For all fissioning nuclei of the main and secondary nucleus chains involved at a given *En*, the fragmentation range used in the PbP treatment (see Ref. 9 and references therein) is constructed by taking a large fragment mass range from symmetric fission up to a very asymmetric split. For each mass number *A* covering this range, three charge numbers *Z* are taken as the nearest integer values above and below the most probable charge $Zp(A)$, which is taken as $Z_{UCD}(A)$ (unchanged charge distribution) corrected with the charge deviation. Available charge polarizations as a function of *A*, $\Delta Z(A)$, or the same average value $\Delta Z = |0.5|$ (with plus sign for light fragments and minus sign for the heavy fragments) for all *A* can be considered together with isobaric charge distributions $p(Z,A)$ taken as Gaussian functions centered on $Zp(A)$ with root-mean-square (rms) as a function of *A*, rms(*A*), or the same average value rms = 0.6 for all *A*. Note that in the absence of ΔZ as a function of *A*, the use of $\Delta Z = |0.5|$ and rms = 0.6 does not change significantly the fragmentation range (i.e., the nuclei *Z, A*, and their isobaric charge distribution); for details see Refs. 10 through 14 and references therein.

The compound nucleus cross sections of the inverse process of prompt neutron evaporation from the nuclei forming the fragmentation ranges of all compound nuclei undergoing fission are provided by optical model calculations using the phenomenological parameterization of Becchetti-Greenlees.[15]

The level density parameters of fragments are calculated in the frame of the superfluid model in which the shell corrections of Möller and Nix[16] and the parameterizations of Ignatiuk[17] for the damping and asymptotic level density parameter were employed. The superfluid level density parameters of fragments are calculated twice, at scission [in the frame of the modeling at scission on which the partition of total excitation energy (TXE) is based[18–20]] and at full acceleration (i.e., at the fragment excitation energies resulting from the TXE partition).

The mass excesses entering the *Q*-values of the fragmentations and the neutron separation energies from fragments are those of the Audi and Wapstra database.[21]

A detailed description of the PbP model of prompt emission can be found in Ref. 9 and references therein.

The total $\nu(A)$ distribution, at a given value of *En*, is obtained by averaging the individual $\nu_i(A)$ distributions [i.e., the $\nu(A)$ corresponding to each compound nucleus undergoing fission at the respective *En*] over the fission probabilities of these compound nuclei, i.e.,

$$\nu(A) = \sum_k \sum_{i=1}^{N^{(k)}} RF_i^{(k)} \nu_i^{(k)}(A) \ . \qquad (4)$$

The individual $\nu_i(A)$ entering Eq. (4) are provided by PbP model calculations performed for each fissioning nucleus *i* at the average excitation energy given by one of Eqs. (1), (2), and (3) according to the way leading to the formation of the respective compound nucleus.

In Eq. (4), (k) denotes the ways that are taken into account at a given *En*, e.g., neutron evaporation from the precursor of the main chain [in this case the average

excitation energies of the compound nuclei are given by Eq. (1)], proton emission from the nuclei of the main chain [leading to compound nuclei of the first secondary chain with average excitation energies given by Eq. (2)], and neutron evaporation from the precursor of the secondary chain [leading to compound nuclei with average excitation energies given by Eq. (3)]. In this relation the index i is running over the nuclei of each chain or way.

In Eq. (4), the fission probabilities are taken as *RF*s. The multichance fission cross sections are provided by nuclear reaction codes (e.g., TALYS, EMPIRE, GNASH) and are usually given in the evaluated nuclear data files (e.g., ENDF, JEFF, JENDL) at least up to the traditional upper energy limit of 20 MeV. At higher *En*, where the secondary nucleus chains are involved, the partial *RF*s corresponding to different ways are also needed (for details see Refs. 4 and 8). In the present paper *RF*s based on the fission cross sections of the ENDF/B-VIII evaluation[6] are used, allowing one to provide the total $\nu(A)$ of n + ^{235}U and n + ^{239}Pu up to En = 20 MeV. Individual $\nu(A)$ results at *En* above 20 MeV, including the secondary nucleus chain and ways [with average excitation energies of the fissioning compound nuclei given by Eqs. (2) and (3)], as well as total $\nu(A)$ results (based on *RF* from our own neutron-induced cross-section calculation above 20 MeV) are exemplified, too.

The existence of experimental $\nu(A)$ data at *En* below the threshold of the second-chance fission, i.e., at thermal *En* for both ^{235}U(n_{th},f) and ^{239}Pu(n_{th},f) and at *En* of 0.5 and 5.5 MeV for ^{235}U(n,f), allows a direct validation by the comparison of calculated $\nu(A)$ with these data.

An indirect validation of total $\nu(A)$ is possible because the average number of prompt neutrons emitted from fission fragments $\langle\nu\rangle_{FF}$, obtained by averaging the individual $\nu(A)$ over $Y(A)$, is strongly dependent on the $\nu(A)$ distribution while the $Y(A)$ distribution has only a very weak influence.[4,5] On the other hand, the only experimental data available in a large amount, for many neutron-induced reactions of actinides and over a large *En* range, refer to the total average prompt neutron number $\langle\nu\rangle_{tot}$. At *En* below the second-chance fission, $\langle\nu\rangle_{tot}$ experimentally measured is just the average number of prompt neutrons emitted by fission fragments $\langle\nu\rangle_{FF}$. At higher *En*, $\langle\nu\rangle_{tot}$ is the sum of $\langle\nu\rangle_{FF}$ (emitted by fission fragments) and the total number of neutrons emitted before fission, usually named prefission neutrons $\langle\nu\rangle_{prefiss}$. At *En* where multichance fission occurs, both $\langle\nu\rangle_{FF}$ and $\langle\nu\rangle_{prefiss}$ are dependent on the nuclear reaction calculations. If evaluated nuclear reaction data from recently released evaluated nuclear data libraries are used, then a good description of experimental $\langle\nu\rangle_{tot}$ data by the calculated $\langle\nu\rangle_{tot}$ can be considered as an indirect validation[4,5] of total $\nu(A)$ given by Eq. (4). This indirect validation can provide valuable indications especially concerning the magnitude of the predicted total $\nu(A)$ and less concerning its shape.

Note that the individual $\nu(A)$ provided by the PbP model at a given *En* [i.e., $\nu(A)$ of each compound nucleus undergoing fission calculated at its average excitation energy given by Eqs. (1), (2), and (3)] remains valid irrespective of the fission probabilities employed to predict the total $\nu(A)$. Consequently, the individual $\nu(A)$ of PbP can be used with different *RF*s based on more recent and/or more refined nuclear reaction calculations.

III. RESULTS AND DISCUSSION

III.A. PbP Results of $\nu(A)$ at *En* Below the Threshold of the Second-Chance Fission

The PbP results of $\nu(A)$ for ^{235}U(n,f) at *En* where only one fission chance is involved were already reported. They describe well the existing experimental data at thermal *En* as reported in Ref. 9 and also at 0.5 and 5.5 MeV; see Refs. 10 and 18. For this reason, in Fig. 1 only the PbP result of $\nu(A)$ for ^{239}Pu(n_{th},f) is given (full red circles) in comparison with the experimental data[22–26] taken from EXFOR (Ref. 27) (different open symbols and symbols with a cross inside colored in black and gray) and the $\nu(A)$ result of GEF (Ref. 7) (full blue diamonds). It can be seen that both $\nu(A)$ results of PbP and GEF are in overall good agreement with the experimental data.

The PbP result of $\nu(A)$ gives an excellent description of the experimental data of Fraser and Milton[26] (squares with a cross inside) at A above 130. It is known that the prompt neutron multiplicity always exhibits a pronounced minimum at A around 130 (due to the magic and double magic heavy fragments with N = 82 and Z = 50). The $\nu(A)$ result of PbP exhibits a minimum at A of about 130, too. The experimental data also exhibit a minimum at A around 130, except the data of Fraser and Milton[26] for which the minimum is shifted at $A_H \sim 126$. The minimum at $A_H \sim 130$ exhibited by $\nu(A)$ of PbP is in agreement with the data of Nishio et al.,[24] Apalin et al.,[25] and Batenkov et al.,[22] and it is more pronounced than the minimum of the GEF result, which is visibly higher and exhibits almost constant values at A_H between 127 and 133 (in agreement only with three data points of Tsuchiya et al.[23]). The $\nu(A)$ of PbP slowly overestimates the

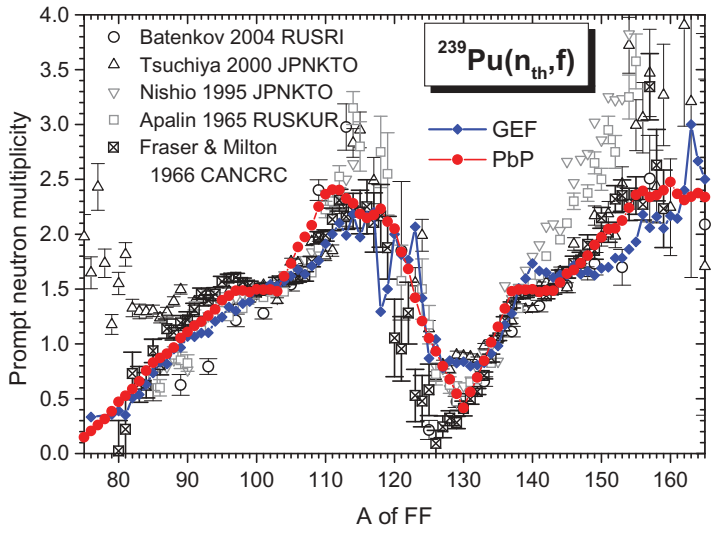

Fig. 1. Prompt neutron multiplicity distribution $\nu(A)$ of ^{239}Pu(n_{th},f): the PbP result (full red circles) in comparison with the experimental data (different black and gray open symbols and symbols with a cross inside) and the result of GEF (full blue diamonds).

experimental data at A_L between 105 and 109, while the GEF result describes well these data. Also, it can be seen that the data of Fraser and Milton (and other data, too) exhibit a plateau at A_L around 97 and another plateau at A_H between 137 and 144. The PbP result exhibits and reproduces these two plateaus. At A_H above 140 and A_L near symmetry (between 115 and 120), the data of Nishio et al.[24] and Apalin et al.[25] (open gray down triangles and squares, respectively) are much higher than the other data that are not described by our result nor by the result of GEF. At A above 147, the $\nu(A)$ of GEF underestimates all experimental data.

The existing experimental $\nu(A)$ data of spontaneous fission and neutron-induced fission at low En exhibit a systematic behavior of the ratio $\nu_H/(\nu_L + \nu_H)$ as a function of A_H. This behavior (mentioned by Wahl[28] and in our previous papers, e.g., Refs. 9, 10, and 11) consists of a ratio less than 0.5 for A_H going from symmetric fission up to about the most probable fragmentation ($A_H \sim 140$ for the majority of fissioning nuclei) with a minimum placed around 130 (due to the magic heavy fragments with $N = 82$ and/or $Z = 50$). At A_H above ~140, the ratio becomes higher than 0.5, and it exhibits an almost linear increase with A_H. In the absence of experimental $\nu(A)$ data, the verification if a calculated $\nu(A)$ accomplishes the systematic behavior of the ratio ν_H/ν_{pair} as a function of A_H can be a validation, too. Such ν_H/ν_{pair} ratios as a function of A_H are illustrated in Fig. 2 for ^{235}U(n,f) at (a) thermal En, (b) at 0.5 and 5.5 MeV, and (c) for ^{239}Pu(n_{th},f). The PbP results are plotted with full circles or circles with a cross inside, the GEF results are plotted with blue diamonds or diamonds with a cross inside, and the experimental data[22–27,29–36] are plotted with different open symbols or squares with a cross inside. As can be seen, the behavior of the ν_H/ν_{pair} ratio as a function of A_H is reproduced by both calculations. However, it can be observed that the ν_H/ν_{pair} ratio of GEF becomes higher than 0.5 at A_H around 122 in the case of ^{239}Pu(n_{th},f) and around 123 to 124 in the case of ^{235}U(n_{th},f). This fact contradicts the systematic behavior of all experimental ratios $\nu_H/\nu_{pair}(A_H)$ at low energies (especially at thermal En), which always show ν_H/ν_{pair} ratios less than 0.5 at A_H going from symmetric fission up to about 140 (i.e., in this A_H range, the light fragments emit more neutrons than the complementary heavy fragments).

The PbP model results of $\nu(A)$ at En below the threshold of the second-chance fission are exemplified for six values of En in Fig. 3b. The $\nu(A)$ results of GEF at the same En values are given in Fig. 3a (with the same symbols as the corresponding PbP results). It is easy to see that the $\nu(A)$ shapes of PbP and GEF are different. Another feature of $\nu(A)$ consisting of the prompt multiplicity increase with En mainly for heavy fragments is observed in both calculations. This increase of $\nu(A)$ for heavy fragments is more pronounced in the case of GEF. The minimum of $\nu(A)$ at A around 130 is more pronounced in the case of PbP.

Note that the values of the En at which $\nu(A)$ of ^{239}Pu(n,f) are plotted in Fig. 3 are those where experimental $Y(A)$ data[37] exist in the EXFOR database,[38] allowing

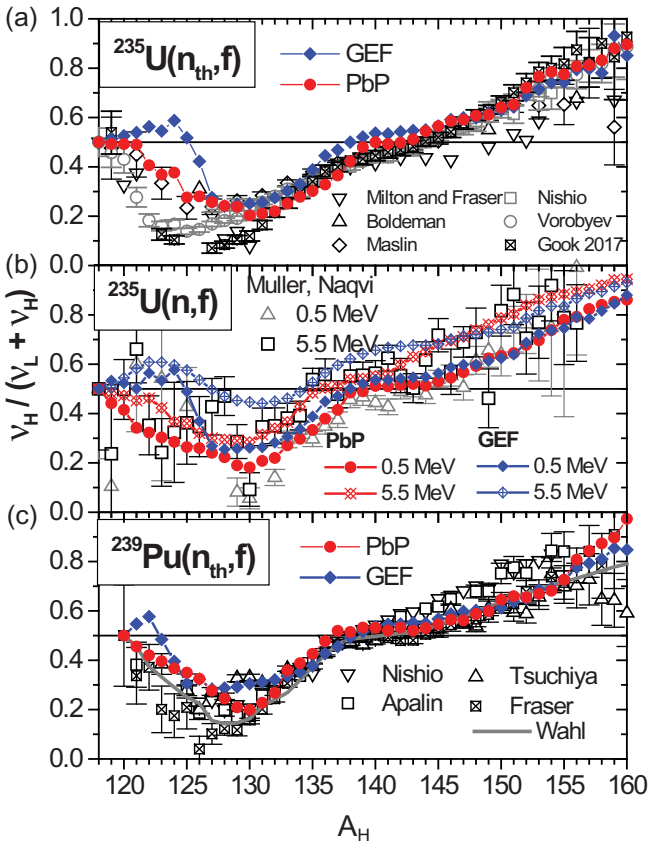

Fig. 2. The ratio ν_H/ν_{pair} as a function of A_H of ^{235}U(n,f) at (a) thermal En and (b) at En = 0.5 and 5.5 MeV and (c) of ^{239}Pu(n_{th},f); the results of PbP (full circles or circles with a cross inside) and GEF (full diamonds or diamonds with a cross inside) in comparison with the experimental data (different open symbols or with a cross inside).

one to calculate the total average number of prompt neutrons.

The total average number of prompt neutrons (which are emitted only by fragments when En is below the threshold of the second-chance fission, i.e., $\langle\nu\rangle_{tot} = \langle\nu\rangle_{FF}$) is calculated by averaging the $\nu(A)$ distributions of PbP and GEF over experimental $Y(A)$ distributions[38–40] and over $Y(A)$ provided by the GEF code.[7] Note that differences between the experimental $Y(A)$ data and the $Y(A)$ of GEF exist; they are significant at all En in the case of ^{239}Pu(n,f), while for ^{235}U(n,f), the $Y(A)$ of GEF give an overall description of the experimental data.

Results of the total average number of prompt neutrons as a function of En are given in Fig. 4 [^{235}U(n,f) in Fig. 4a and ^{239}Pu(n,f) in Fig. 4b] in comparison with the experimental data retrieved from EXFOR (Refs. 41 through 85) (different open symbols). The plotted $\langle\nu\rangle_{tot}$ are obtained as follows: by averaging $\nu(A)$ of PbP over the experimental $Y(A)$ (full red circles) and over the $Y(A)$ of GEF (full orange up triangles) and by averaging $\nu(A)$ of GEF over the experimental $Y(A)$ (full green down triangles) and over $Y(A)$ of GEF (full blue diamonds). The very close values of $\langle\nu\rangle_{tot}$ obtained by averaging the same $\nu(A)$ distribution over two different $Y(A)$ are easily seen (full red circles and orange up triangles on one hand; full blue diamonds and green down triangles on the other hand). This fact proves again that the average number of prompt neutrons emitted by fragments $\langle\nu\rangle_{FF}$ is strongly dependent on the $\nu(A)$ distribution while the $Y(A)$ distribution has only a weak influence (as demonstrated in Fig. 4 and Refs. 4 and 5). Consequently, it can be used as an indirect validation of the $\nu(A)$ distribution in the absence of experimental $\nu(A)$ data.

As can be seen in Fig. 4a, in the case of ^{235}U(n,f), the $\langle\nu\rangle_{tot}$ result of GEF at En above 1 MeV overestimates the experimental data and the PbP result. The difference between the $\langle\nu\rangle_{tot}$ results of PbP and GEF is of 7% at En = 3 MeV and about 5% at other En.

In the case of ^{239}Pu(n,f) (Fig. 4b), the $\langle\nu\rangle_{tot}$ results of PbP and GEF are close to each other (the differences being less than 2%), and both describe well the experimental data.

Note that looking at Fig. 3, it can be seen that the $\nu(A)$ shapes of PbP and GEF are different. The shape of $\nu(A)$ distributions provided by each of these models does not vary too much from one En to another. The magnitudes of $\nu(A)$ provided by PbP and GEF are almost the same in the case of ^{239}Pu(n,f) (leading to the close $\langle\nu\rangle_{tot}$ results of PbP and GEF given in Fig. 4b), and they are different in the case of ^{235}U(n,f) (leading to the visible differences between the $\langle\nu\rangle_{tot}$ results of PbP and GEF given in Fig. 4a). In other words the indirect validation of $\nu(A)$, by the comparison of $\langle\nu\rangle_{tot}$ with experimental data, gives valuable indications especially about the magnitude of $\nu(A)$ and less about its shape.

III.B. PbP Calculation of $\nu(A)$ in the En Range of Multichance Fission

Examples of PbP calculations at En where multichance fission occurs are given in Fig. 5. The individual $\nu(A)$ corresponding to the compound nuclei undergoing fission at each En are plotted with open symbols. Note that at En up to 20 MeV, only the prompt emission from compound nuclei of the main chain are taken into account, i.e., $^{236–233}$U and $^{240–237}$Pu.

Regarding the evolution of the individual $\nu(A)$ shape with increasing En, a less pronounced sawtooth shape of $\nu(A)$ of the main compound nuclei ^{236}U and

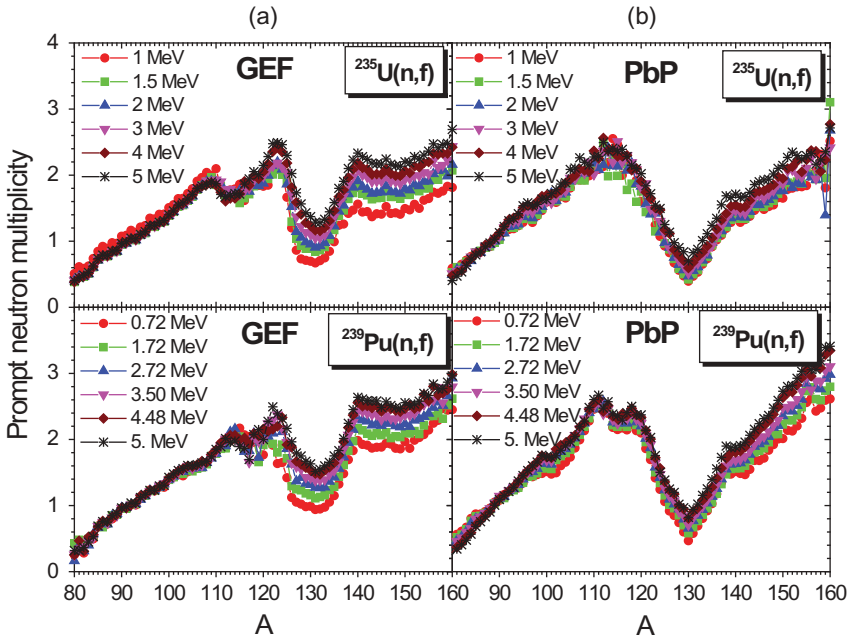

Fig. 3. Prompt neutron multiplicity distribution $\nu(A)$ results of (a) GEF and (b) PbP exemplified at six incident neutron energies covering the range where only the first fission chance is involved.

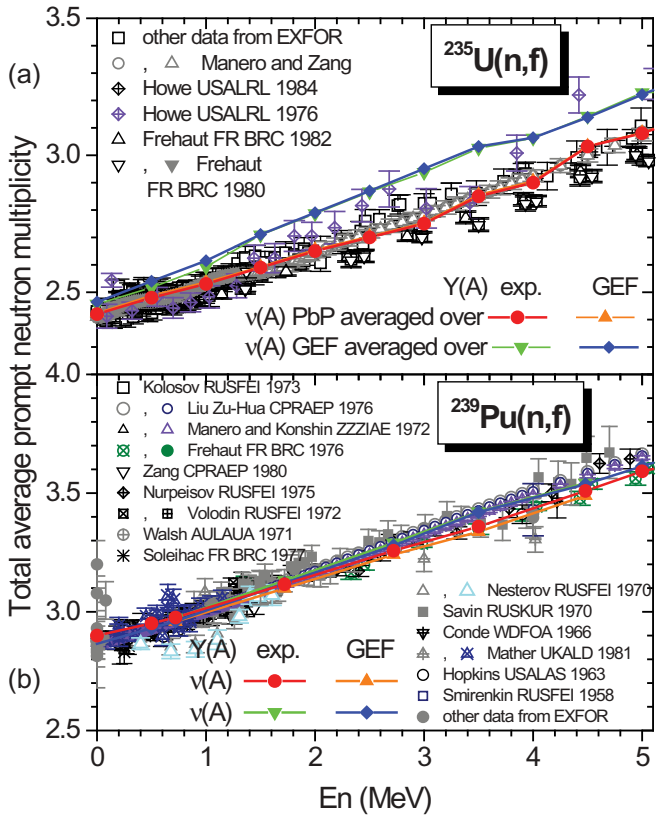

Fig. 4. Total average prompt neutron multiplicity in the *En* range of the first fission chance obtained by averaging the $\nu(A)$ results of PbP and GEF over the experimental $Y(A)$ data and over $Y(A)$ of GEF (full red, blue, orange, and green symbols) in comparison with the experimental data from EXFOR (different open symbols and symbols with a cross inside colored in black, gray, olive, and violet and full symbols colored in olive and gray).

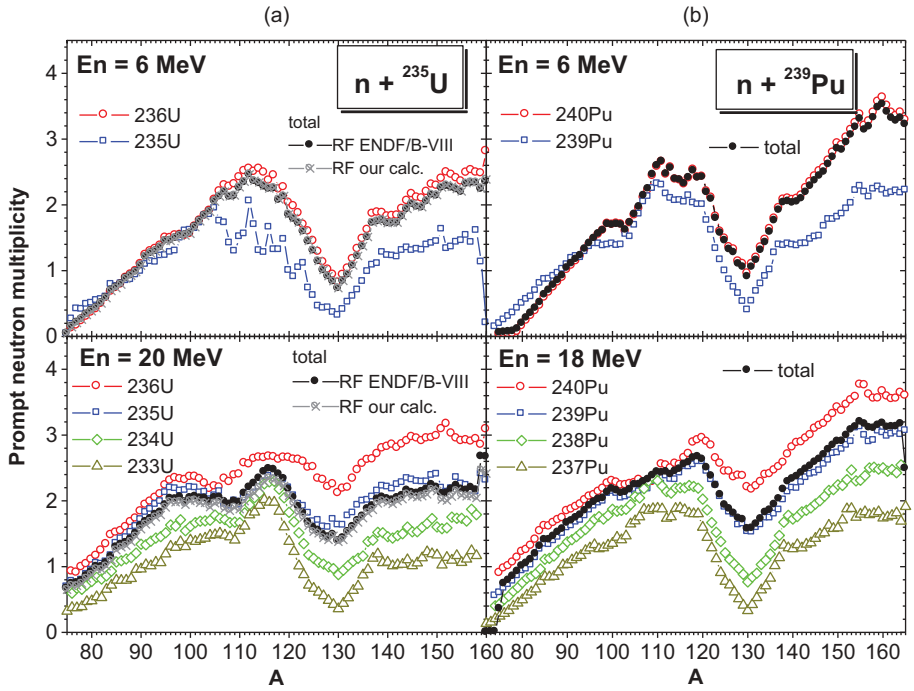

Fig. 5. Individual $\nu(A)$ (open symbols) and total $\nu(A)$ (full circles and circles with a cross inside) for the neutron-induced fission of (a) ^{235}U and (b) ^{239}Pu exemplified for each reaction at two incident neutron energies (En = 6 MeV for both reactions, En = 20 MeV for n + ^{235}U and En = 18 MeV for n + ^{239}Pu).

^{240}Pu (open red circles), having the highest average excitation energy, is observed. The average excitation energy of the other compound nuclei being lower, the corresponding individual $\nu(A)$ do not show significant changes of the sawtooth shape with increasing En. Consequently, the shape of the total $\nu(A)$, as a superposition of individual $\nu(A)$ shapes weighted with RF, does not show significant changes of the sawtooth character. This kind of changes in shape and the tendency to an almost linear behavior occur at much higher En than 20 MeV (see, e.g., Ref. 4).

The total $\nu(A)$ plotted in Fig. 5 with full black circles are obtained by averaging the individual $\nu(A)$ over the RFs of the ENDF/B-VIII evaluations[6] according to Eq. (4). These RFs are plotted in Fig. 6 with solid red lines, together with RF of the JENDL4 evaluation[86] (blue dash-dotted

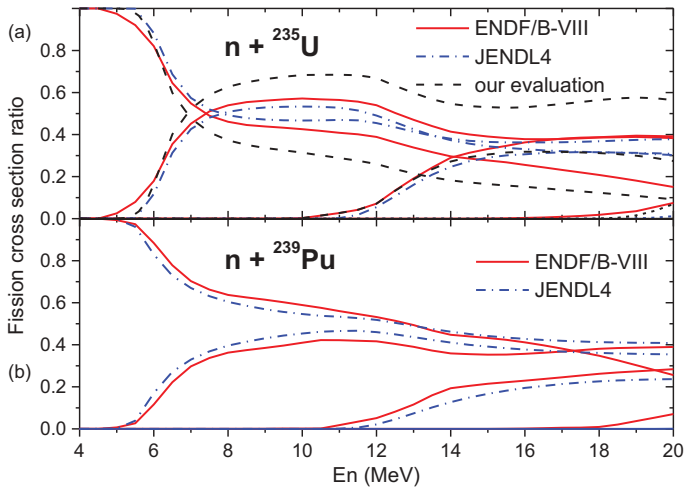

Fig. 6. Fission cross-section ratio of (a) n + ^{235}U and (b) n + ^{239}Pu of the evaluations ENDF/B-VIII (solid lines) and JENDL4 (dash-dotted lines). The RFs from our neutron-induced cross-section calculation for n + ^{235}U are plotted with dashed lines.

lines) and *RF* of our neutron-induced cross-section calculation performed for ^{235}U up to 50 MeV (black dashed lines). This calculation is based on the fission model with subbarrier effects implemented in an improved version of the GNASH code, used for the neutron-induced cross-section calculations of many actinides. Details about the modeling, the prescriptions, and the parameters used can be found in, e.g., Refs. 87 through 90 and references therein. As can be seen in Fig. 6, for both reactions, *RF*s of ENDF/B-VIII and JENDL4 do not differ much from each other. Consequently, the differences between the total $\nu(A)$ based on these *RF*s are insignificant, and only the total $\nu(A)$ obtained with *RF*s of ENDF/B-VIII are plotted with full black circles in Fig. 5. Even if the *RF*s from our evaluation differ visibly from *RF*s of ENDF/B-VII and JENDL4 evaluations, the total $\nu(A)$ based on our *RF*s (plotted in Fig. 5 with gray circles with a cross inside) differ less than 5% from the total $\nu(A)$ based on *RF*s of ENDF/B-VIII. This fact proves again the low sensitivity of total $\nu(A)$ to the *RF*s of different calculations, already discussed in Ref. 4 for the case of n + ^{238}U.

A comparison of total $\nu(A)$ results of PbP (full circles) and GEF (open squares) at eight *En* covering the range from 6 to 20 MeV is illustrated in Figs. 7a and 7b. As can be seen in the case of n + ^{235}U (Fig. 7a), the total $\nu(A)$ results of PbP and GEF are visibly different in shape and magnitude. The total $\nu(A)$ of GEF are higher and exhibit a pronounced increase at A around 122 to 124. This increase can be interrelated with the behavior of the individual ν_H/ν_{pair} ratios of GEF, which exhibit an increase above 0.5 at these A values (i.e., the heavy fragments emitting more

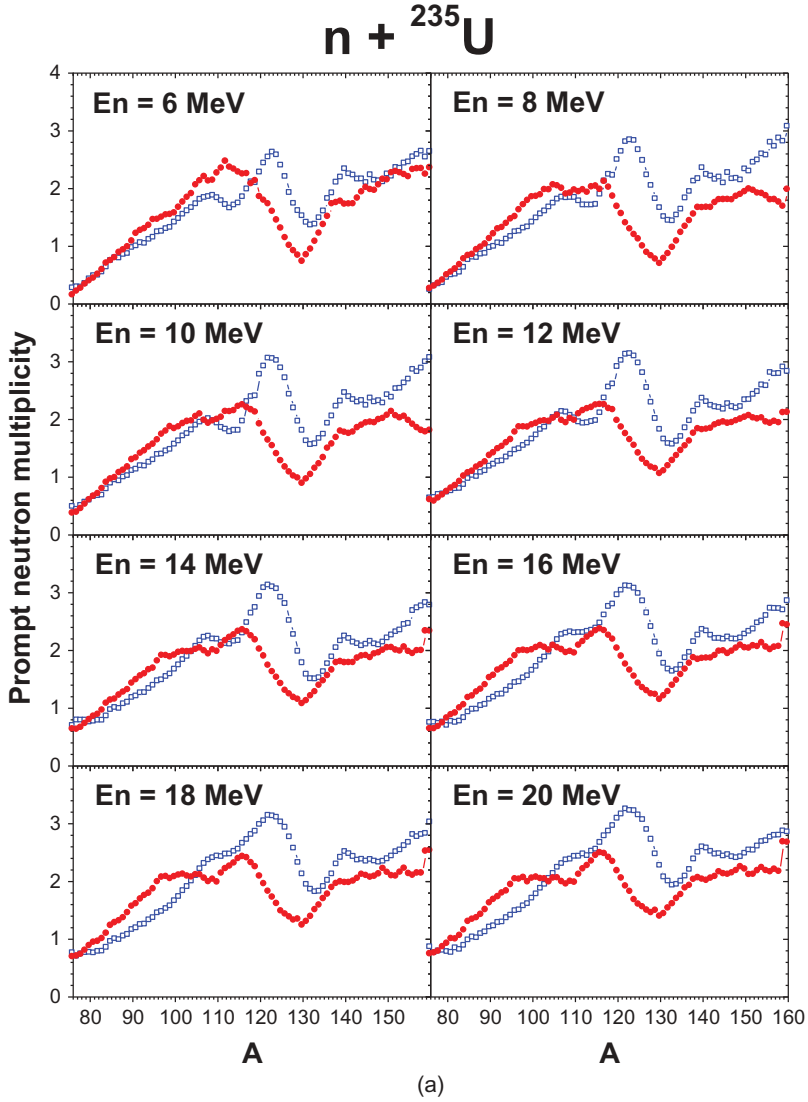

Fig. 7. Total $\nu(A)$ of (a) n + ^{235}U and (b) n + ^{239}Pu, at eight incident neutron energies ranging from 6 to 20 MeV. The results of PbP are plotted with full circles and those of GEF with open squares.

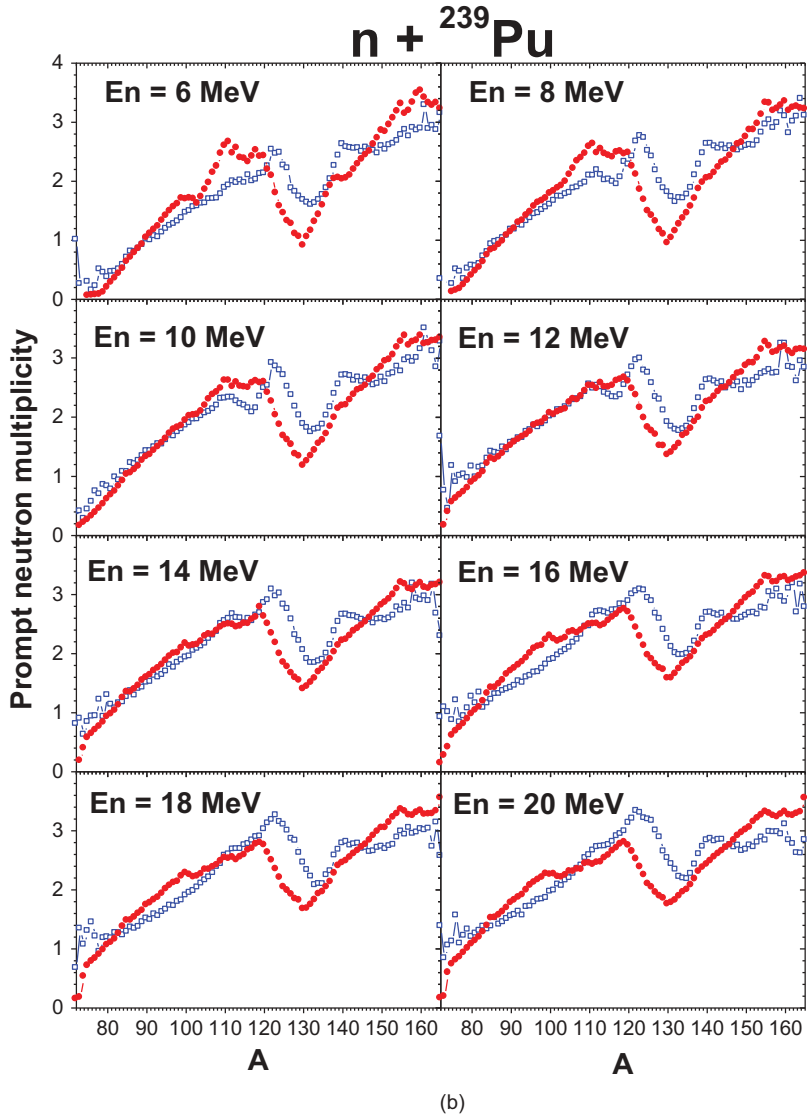

Fig. 7. (Continued).

neutrons than the complementary light fragments) as can be seen in Fig. 2. Consequently, the GEF results of total $\nu(A)$ as a superposition of individual $\nu(A)$ of several compound nuclei exhibit a pronounced increase at A around 122 to 124, too.

Compared to the reactions n + $^{235,\ 238}$U when large differences between the predicted $\nu(A)$ of PbP and GEF occur, in the case of n + ^{239}Pu, the total $\nu(A)$ results of PbP and GEF are much closer; see Fig. 7b. Differences in shape between the total $\nu(A)$ results of PbP and GEF appear only at A between 120 and 140.

An indirect validation of predicted total $\nu(A)$, at En where multiple fission chances occur, is also possible via the total average number of prompt neutrons $\langle\nu\rangle_{tot}$, which can be compared with experimental data.

The average number of prompt neutrons emitted by fragments $\langle\nu\rangle_{FF}$ can be obtained by averaging the total $\nu(A)$ of PbP over available $Y(A)$ distributions above the threshold of the second-chance fission. Such $Y(A)$ distributions are provided by the code GEF (Ref. 7). Taking into account that $\langle\nu\rangle_{FF}$ is strongly dependent on the $\nu(A)$ distribution and $Y(A)$ has only a very low influence (as demonstrated in Fig. 4 and Refs. 4 and 5), the obtained values of $\langle\nu\rangle_{FF}$ can reflect well the $\nu(A)$ prediction. They are plotted with red stars in Fig. 8a for n + ^{235}U and Fig. 8b for n + ^{239}Pu. The average number of prefission neutrons $\langle\nu\rangle_{prefiss}$ is plotted with red circles with a cross inside, and the total average number of neutrons $\langle\nu\rangle_{tot}$ (as a sum of $\langle\nu\rangle_{FF}$ and $\langle\nu\rangle_{prefiss}$) is plotted with full red circles. The GEF results of $\langle\nu\rangle_{FF}$,

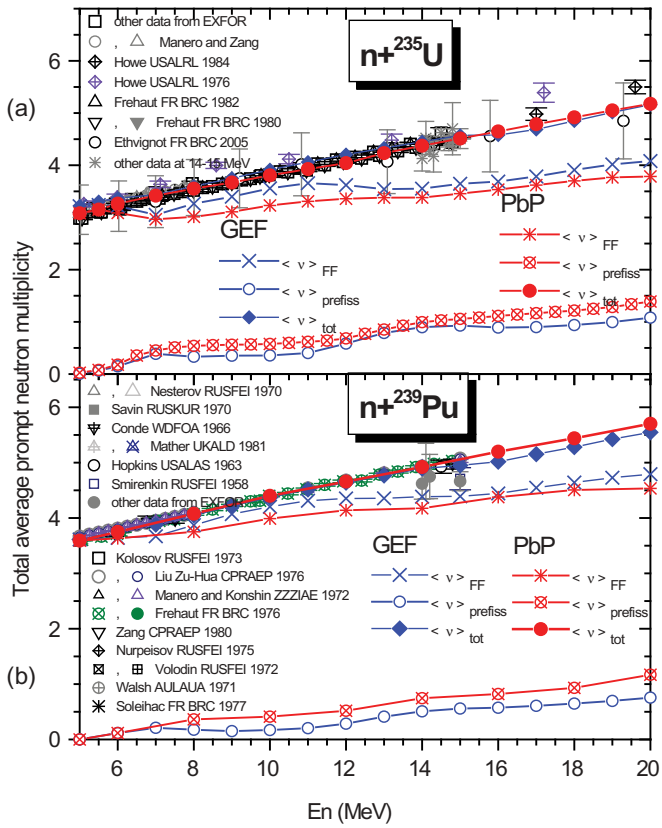

Fig. 8. Total average number of prompt neutrons $\langle\nu\rangle_{tot}$ of PbP (full circles) and GEF (full diamonds), $\langle\nu\rangle_{FF}$ of PbP (stars) and GEF (crosses), and $\langle\nu\rangle_{prefiss}$ of PbP (circles with a cross inside) and GEF (open circles) as a function of *En* for (a) n + ^{235}U and (b) n + ^{239}Pu. The present results are in red color and the GEF results in blue color. The experimental data are plotted with different symbols (colored in black, olive, violet, and gray).

$\langle\nu\rangle_{prefiss}$, and $\langle\nu\rangle_{tot}$ are also given (blue crosses, open circles, and circles with a cross inside, respectively). The experimental $\langle\nu\rangle_{tot}$ data[43–85] taken from EXFOR (Refs. 41 and 42) are given with different black and gray open symbols and symbols with a cross inside. As can be seen, in the case of n + ^{235}U, $\langle\nu\rangle_{tot}$ of PbP describes well the experimental data over the entire *En* range. The $\langle\nu\rangle_{tot}$ result of GEF slightly overestimates the majority of the experimental data up to about 15 MeV. Above this energy, $\langle\nu\rangle_{tot}$ of GEF becomes a little bit lower than the PbP result.

In the case of n + ^{239}Pu, the $\langle\nu\rangle_{tot}$ results of PbP and GEF are close to each other and describe well the experimental data, which exist up to 14.5 MeV. Above this energy, again $\langle\nu\rangle_{tot}$ of GEF becomes lower than the PbP result. The differences between the $\langle\nu\rangle_{tot}$ results of PbP and GEF above 15 MeV are higher in the case of ^{239}Pu than for ^{235}U. Above 15 MeV, the present result of $\langle\nu\rangle_{tot}$ keeps the same increasing trend, which is also in agreement with the recent evaluations ENDF/B-VIII (Ref. 91), JENDL4 (Ref. 92), and JEFF3.2 (Ref. 93).

Concerning the components of $\langle\nu\rangle_{tot}$, in both cases as well as in the previous studied case of n + ^{238}U (Ref. 4), the $\langle\nu\rangle_{FF}$ results of GEF are higher than those of PbP. The compensation effect between the components $\langle\nu\rangle_{FF}$ and $\langle\nu\rangle_{prefiss}$ of GEF works well in the case of n + ^{239}Pu leading to a result of $\langle\nu\rangle_{tot}$, which is in good agreement with the experimental data up to about 15 MeV.

PbP calculations of individual $\nu(A)$ (i.e., corresponding to each compound nucleus of the main chain and of the secondary nucleus chains formed by charged particle emission) can be performed at any *En* above 20 MeV. The total $\nu(A)$, depending on the total and partial *RF*s, can be predicted only if neutron-induced cross-section calculations are available above 20 MeV.

Examples of PbP results of individual $\nu(A)$ of the main U chain (open symbols) and Pa secondary chain (solid lines) at four *En* above 20 MeV are given for n + ^{235}U in Fig. 9. The change in shape of individual $\nu(A)$ with increasing *En*, i.e., a less pronounced sawtooth character, is visible especially for the main compound nucleus ^{236}U, which has the highest average excitation energy. See the open circles in each frame of Fig. 9.

The individual $\nu(A)$ of ^{236}U at *En* = 50 MeV (plotted with open circles in the lower frame of Fig. 9b) exhibits an almost linear increase (except the *A* region 120 to 135), and it can be fitted well. This individual $\nu(A)$ is plotted with open red circles in Fig. 10 together with its linear fit (a red solid line).

At limit when an individual $\nu(A)$ is taken linear, i.e., $\nu(A) = \alpha A + \beta$, the corresponding prompt neutron multiplicity of a mass pair (A_L + A_H = A_0) becomes constant (independent of *A*), i.e., $\nu_{pair} = \alpha A_0 + 2\beta$. The linear fit of $\nu(A)$ plotted with a solid line in Fig. 10 leads to the ν_{pair} value of 7.461 (indicated by a horizontal black line), which approximates very well the calculated $\nu_{pair}(A)$ of ^{236}U plotted with open squares in Fig. 10.

The almost linear increasing behavior of the individual $\nu(A)$ at high excitation energies of the fissioning nuclei (i.e., the main compound nuclei at high *En*, above 40 to 50 MeV) is due to the excitation energies of fully accelerated fragments (E^*) coming from these fissioning nuclei, which also exhibit an almost linear increase with the fragment mass number *A*. This almost linear shape of $E^*(A)$ at high excitation energies of a fissioning nucleus is the consequence of the vanishing of shell effects entering the superfluid expression of

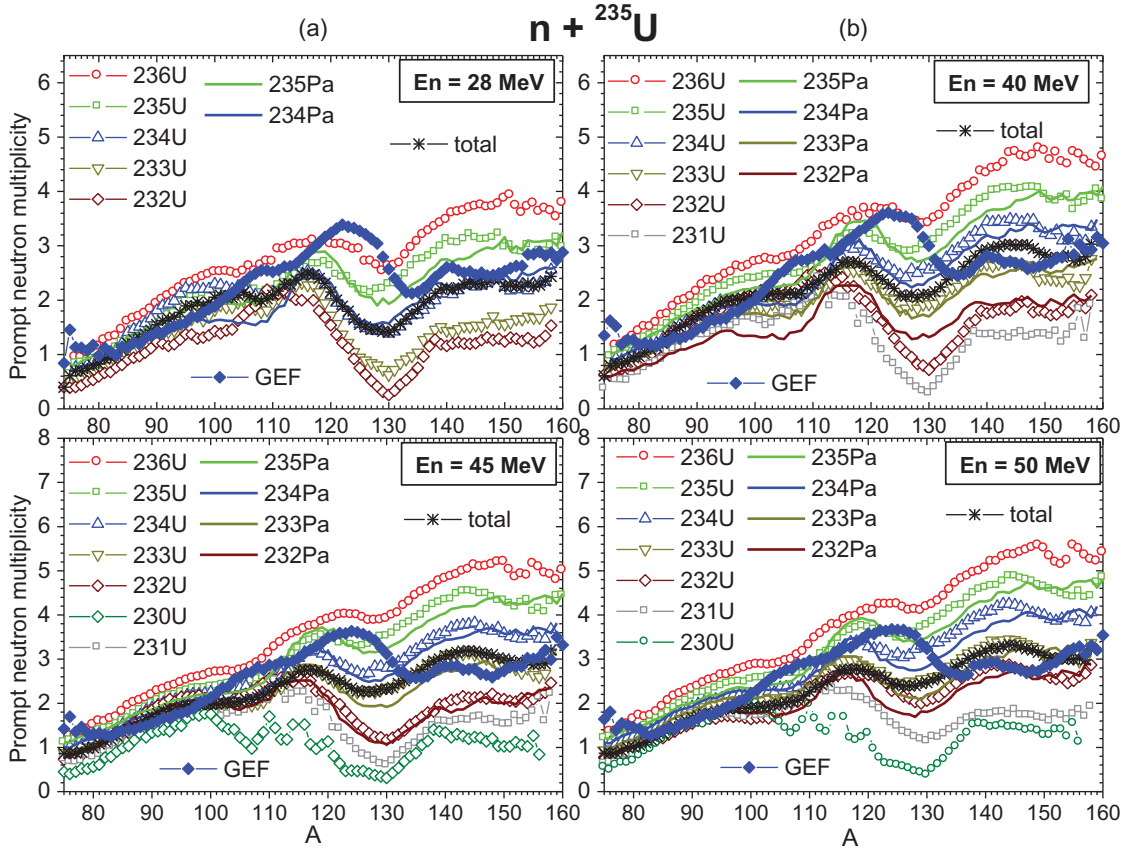

Fig. 9. Individual $\nu(A)$ corresponding to the fissioning nuclei of the main U chain (open symbols) and of the secondary Pa chain (solid lines). The total $\nu(A)$ obtained by averaging these individual $\nu(A)$ over *RF* of our evaluation is given with stars. The total $\nu(A)$ provided by the GEF code are given with full diamonds.

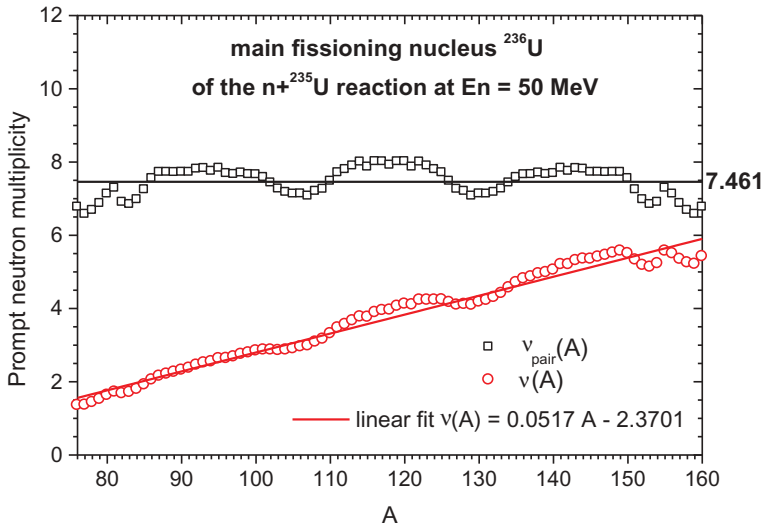

Fig. 10. Individual $\nu(A)$ of the main fissioning nucleus ^{236}U at En = 50 MeV (open circles) and its linear fit (solid red line); the corresponding $\nu_{pair}(A)$ is plotted with open squares. The constant value ν_{pair} = 7.461 resulting from the linear fit of $\nu(A)$ is indicated with a horizontal line.

fragment level density parameters that are involved in the modeling at scission on which the TXE partition is based.[4,18,19]

The PbP calculations of individual $\nu(A)$ at high excitation energies of the fissioning nuclei, performed for the compound nuclei involved in three neutron-induced reactions n + ^{238}U

(Ref. 4), n + ^{235}U, and n + ^{239}Pu (this work), allow one to emphasize interesting systematic behaviors of the prompt neutron multiplicity distributions $\nu(A)$, $\nu_{pair}(A)$ and of the ratio $\nu_H/\nu_{pair}(A_H)$ with increasing energy.

Such systematic behaviors can be illustrated by schematic representations of the shapes of individual $\nu(A)$ and $\nu_{pair}(A)$ and their evolution with increasing energy (i.e., simplified shapes by connected line segments). An example is given in Fig. 11 for the main fissioning nucleus ^{236}U of the reaction n + ^{235}U: (a) the qualitative schematic representation of $\nu(A)$ and (b) of $\nu_{pair}(A_H)$.

In Fig. 11a, three examples of simplified schematic representations of $\nu(A)$ at En below the threshold of the second-chance fission are illustrated by the solid red, dashed dark yellow, and dotted cyan lines. With increasing En, the sawtooth shape of $\nu(A)$ becomes less pronounced, this behavior being illustrated by the gray dash-dotted and wine dash double dotted lines, which correspond to En of about 10 and 20 MeV, respectively. At higher En (where many fissioning nuclei of the main and secondary nucleus chains are involved), the sawtooth shape of individual $\nu(A)$

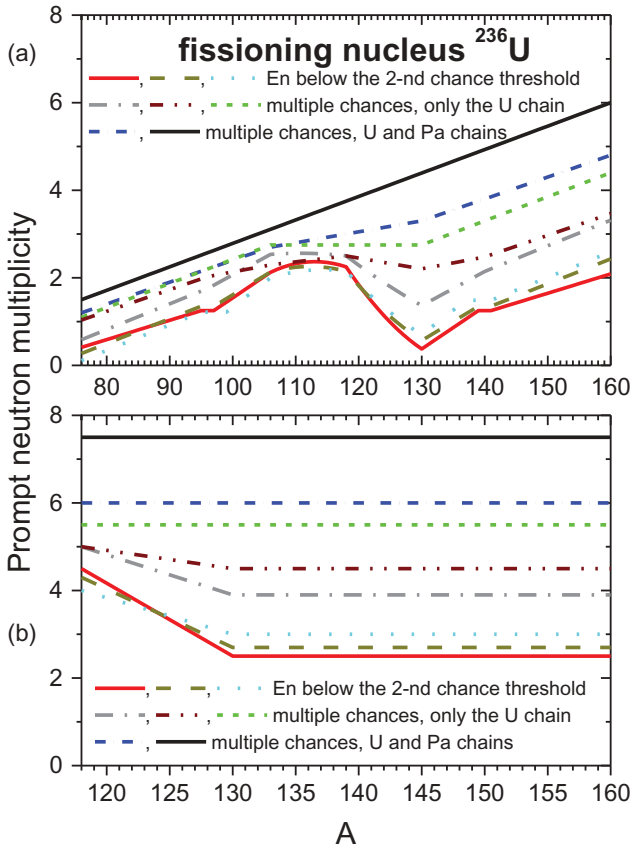

Fig. 11. Schematic representation of the evolution of the shapes of (a) $\nu(A)$ and (b) $\nu_{pair}(A)$ with increasing En, illustrated for the main fissioning nucleus ^{236}U of the reaction n + ^{235}U.

corresponding to the first few compound nuclei is washing out, arriving to an almost linear increase. This behavior is schematically illustrated by the blue short dashed and the black solid line.

It is known that the prompt neutron multiplicity of fragment mass pair $\nu_{pair}(A)$ is almost constant over the fragment mass range except the near-symmetric region where it is higher. This behavior of ν_{pair} as a function of A_H is qualitatively illustrated in Fig. 11b, using the same type of lines as the corresponding schematic $\nu(A)$ given in Fig. 11a. The solid red, dashed dark yellow, and dotted cyan lines illustrate $\nu_{pair}(A)$ at En below the threshold of the second-chance fission. The gray dash-dotted and wine dash double dotted lines are the schematic representation of $\nu_{pair}(A)$ for En where three to four fission chances are involved (up to 20 MeV). With increasing En, i.e., the increasing average excitation energy of the main compound nucleus, its $\nu_{pair}(A)$ tends to be constant over the entire fragment mass range including the region near symmetry, too. See the green short dashed, blue short dash dotted line and the solid black line corresponding to En ranging from about 25 to 50 MeV or even higher values.

Note that similar schematic representations of $\nu(A)$ and $\nu_{pair}(A)$ can be plotted also for other fissioning nuclei by shifting the A range.

The systematic behaviors of $\nu(A)$ and $\nu_{pair}(A)$ mentioned above have as consequence the evolution with increasing energy of the ratio ν_H/ν_{pair} as a function of A_H, which was schematically illustrated in Ref. 4 for the main fissioning nucleus ^{239}U. The shape of $\nu_H/\nu_{pair}(A_H)$ evolves from the behavior at low En described in Sec. III.A (Fig. 2) up to an almost linear increase at high En, with a lower slope than of $\nu(A)$. At the limit when $\nu(A) = \alpha A + \beta$ and ν_{pair} is a constant equal to $\alpha A_0 + 2\beta$, the ratio ν_H/ν_{pair} as a function of A_H becomes linear, too.

As an exercise, total $\nu(A)$ can be calculated by using the RF of our evaluation. Examples of such total $\nu(A)$ of n + ^{235}U at En above 20 MeV are given with black stars in Fig. 9. The total $\nu(A)$ of GEF are also plotted with full blue diamonds. Significant differences in shape and magnitude between the total $\nu(A)$ results of GEF and PbP are visible.

A comparison of the present results of $\langle\nu\rangle_{FF}$, $\langle\nu\rangle_{prefiss}$, and $\langle\nu\rangle_{tot}$ with the results of GEF and the experimental data is given in Fig. 12 (using the same symbols and colors as in Fig. 8).

Note that our $\langle\nu\rangle_{prefiss}$ result (plotted in Fig. 12 with red circles with a cross inside) includes the preequilibrium component, too.

As can be seen in Fig. 12, the $\langle\nu\rangle_{tot}$ results of PbP and GEF above 20 MeV are in agreement with the data of Fréhaut[45,46] (down triangles), Ethvignot et al.[47] (open

black circles), and Hove[43] (diamond with a cross inside) taken from the EXFOR library.[41] Even if both $\langle\nu\rangle_{FF}$ and $\langle\nu\rangle_{prefiss}$ of PbP and GEF are different (i.e., $\langle\nu\rangle_{FF}$ of PbP is lower than $\langle\nu\rangle_{FF}$ of GEF, and $\langle\nu\rangle_{prefiss}$ of our calculation is higher than $\langle\nu\rangle_{prefiss}$ of GEF) by a compensation effect in the sum $\langle\nu\rangle_{FF} + \langle\nu\rangle_{prefiss}$, both $\langle\nu\rangle_{tot}$ of PbP and GEF describe the experimental data and do not differ much.

IV. CONCLUSIONS

Postneutron fragment data for the neutron-induced fission of ^{235}U, ^{238}U, and ^{239}Pu at incident energies up to several tens of MeV were measured at LANSCE-WNR. To obtain preneutron fragment distributions, these data need the correction of prompt neutron emission, i.e., the prompt neutron distribution $\nu(A)$. The lack of experimental $\nu(A)$ data at *En* where the multichance fission occurs imposes the use of $\nu(A)$ predicted by prompt emission models.

The PbP model of prompt emission has answered to this request by the prediction of total $\nu(A)$ for the reaction n + ^{238}U in Ref. 4 and for the reactions n + ^{235}U and n + ^{239}Pu in the present work.

The individual $\nu(A)$ distributions corresponding to each compound nucleus undergoing fission of the main and secondary nucleus chains can be provided by the PbP model at any *En* where multiple fission chances are involved.

The total $\nu(A)$ distribution is obtained by averaging these individual $\nu(A)$ over the fission probabilities of the compound nuclei formed at a given *En*. These fission probabilities can be expressed as total and partial *RFs*. These *RFs* can be obtained from neutron-induced cross-section calculations performed either up to the traditional upper *En* limit of 20 MeV (included in the evaluated nuclear data libraries, e.g., ENDF/B, JENDL, JEFF) or up to higher *En* (by taking into account also the fission of compound nuclei of secondary chains formed by charged particle emission). In the present work the *RFs* of the ENDF/B-VIII evaluation are used to obtain the total $\nu(A)$ distributions of both reactions up to 20 MeV.

The PbP results of individual $\nu(A)$ at *En* above 20 MeV are exemplified for the n + ^{235}U reaction up to *En* = 50 MeV.

The PbP calculations for three neutron-induced reactions at incident energies where multiple fission

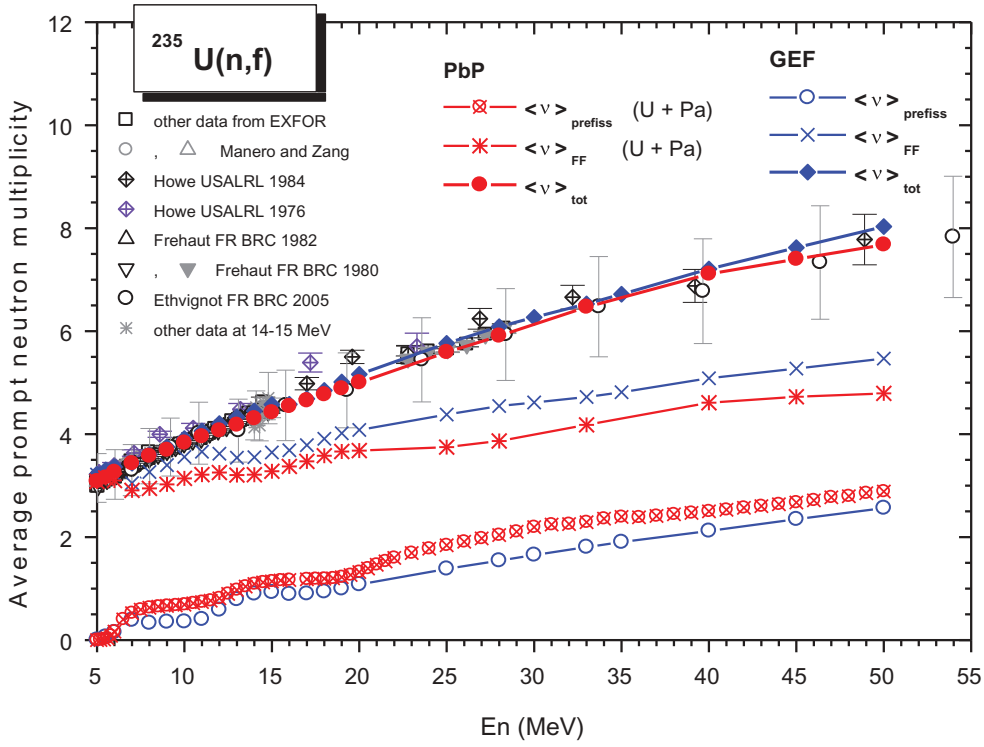

Fig. 12. The $\langle\nu\rangle_{tot}$, $\langle\nu\rangle_{FF}$, and $\langle\nu\rangle_{prefiss}$ results of the present work (full circles, stars and circles with a cross inside, respectively) and of the GEF code (full diamonds, crosses and open circles) for the n + ^{235}U reaction at *En* from 5 to 50 MeV. In the online version the present results are in red color and the GEF results in blue color. The experimental data of $\langle\nu\rangle_{tot}$ are plotted with different symbols (colored in black, violet and gray in the online version).

chances are involved allows one to emphasize the systematic behavior of the shapes of individual prompt neutron distributions $\nu(A)$ and $\nu_{pair}(A)$ with increasing En.

The $\nu(A)$ shape evolves with increasing excitation energy of the fissioning nucleus from a shape with a pronounced sawtooth character at low excitation energies (corresponding to En below the threshold of the second-chance fission) up to an almost linear increasing shape at high excitation energies (corresponding to the first few compound nuclei at En above 40 to 50 MeV).

The prompt neutron multiplicity of fragment mass pair $\nu_{pair}(A)$ at low excitation energies of the fissioning nucleus (i.e., En below the threshold of the second-chance fission) is almost constant over the A range except the near-symmetric region where it is higher. $\nu_{pair}(A)$ of the first few compound nuclei becomes almost constant over the entire fragment mass range at En above 40 to 50 MeV.

In the En range where only one fission chance is involved, the PbP results of $\nu(A)$ for ^{235}U(n,f) and ^{239}Pu(n,f) are directly validated by their very good agreement with the existing experimental data.

An indirect validation of predicted total $\nu(A)$ at any En is possible via the comparison of the total average number of prompt neutrons with the experimental data, which are available in a large amount compared to other prompt emission data, which are scarce or completely missing. This indirect validation is possible because the average number of prompt neutrons emitted by fragments $<\nu>_{FF}$ [obtained by averaging $\nu(A)$ over $Y(A)$] is strongly dependent on the $\nu(A)$ distribution while the $Y(A)$ distribution has only a weak influence.

The present $\nu(A)$ results are compared with the results of the GEF code. In the case of n + ^{235}U, as well as in the previously studied case of n + ^{238}U (Ref. 4), significant differences in shape and magnitude between the predicted $\nu(A)$ of PbP and GEF exist. In the case of n + ^{239}Pu, the predicted $\nu(A)$ of PbP and GEF are closer to each other especially at incident neutron energies between 6 and 14 MeV.

Acknowledgments

A part of this work was done in the frame of the Romanian Exploratory Research Project PCE-2016-0014.

One of the authors (A.T.) acknowledges the short-term visit support by the European Commission within the framework of the CHANDA program.

References

1. D. L. DUKE et al., *EPJ Web of Conf.*, **146**, 04042 (2017); https://doi.org/10.1051/epjconf/201714604042.
2. D. L. DUKE, PhD Thesis, Colorado School of Mines (2015).
3. C. K. MEIERBACHTOL et al., *Phys. Rev. C*, **94**, 034611 (2016); https://doi.org/10.1103/PhysRevC.94.034611.
4. A. TUDORA, F.-J. HAMBSCH, and V. TOBOSARU, *Phys. Rev. C*, **94**, 044601 (2016); https://doi.org/10.1103/PhysRevC.94.044601.
5. A. TUDORA, F.-J. HAMBSCH, and V. TOBOSARU, *EPJ Web of Conf.*, **146**, 04004 (2017); https://doi.org/10.1051/epjconf/201714604004.
6. ENDF/B-VIII Evaluated Nuclear Data Library, Files ZA092235 and ZA094239, MF=3, MT=18, 19, 20, 21, 38, International Atomic Energy Agency Nuclear Data Services; https://www-nds.iaea.org (current as of Feb. 8, 2018).
7. K.-H. SCHMIDT et al., *Nucl. Data Sheets*, **131**, 107 (2016); https://doi.org/10.1016/j.nds.2015.12.009.
8. A. TUDORA, G. VLADUCA, and B. MORILLON, *Nucl. Phys. A*, **740**, 33 (2004); https://doi.org/10.1016/j.nuclphysa.2004.04.112.
9. A. TUDORA and F.-J. HAMBSCH, *Eur. Phys. J. A*, **53**, 159 (2017); https://doi.org/10.1140/epja/i2017-12347-9.
10. A. TUDORA et al., *Nucl. Sci. Eng.*, **181**, *3*, 289 (2015); https://doi.org/10.13182/NSE14-108.
11. R. CAPOTE et al., *Nucl. Data Sheets*, **131**, 1 (2016); https://doi.org/10.1016/j.nds.2015.12.002.
12. A. TUDORA, F.-J. HAMBSCH, and G. GIUBEGA, *Eur. Phys. J. A*, **52**, 182 (2015); https://doi.org/10.1140/epja/i2016-16182-2.
13. A. TUDORA et al., *Rom. Rep. Phys.*, **68**, *2*, 571 (2016).
14. G. GIUBEGA, I. VISAN, and A. TUDORA, *Rom. Rep. Phys.*, **68**, *3*, 1024 (2016).
15. Reference Input Parameter Library IAEA-RIPL3, Segment 4, "Optical Model," IREF = 100 (Becchetti-Greenlees), International Atomic Energy Agency Nuclear Data Services; https://www-nds.iaea.org (current as of Feb. 8, 2018).
16. Reference Input Parameter Library IAEA-RIPL3, Segment 1, "Nuclear Masses and Deformations," Database of Möller and Nix (FRDM), International Atomic Energy Agency Nuclear Data Services.
17. A. V. IGNATIUK, IAEA-RIPL1-TECDOC-1034, Segment V, Chap. 5.1.4, International Atomic Energy Agency Nuclear Data Services (1998).
18. A. TUDORA et al., *Nucl. Phys. A*, **940**, 242 (2015); https://doi.org/10.1016/j.nuclphysa.2015.04.012.

19. C. MORARIU et al., *J. Phys. G Nucl. Part. Phys.*, **39**, *5*, 055103 (2012); https://doi.org/10.1088/0954-3899/39/5/055103.

20. I. VISAN, G. GIUBEGA, and A. TUDORA, *Rom. Rep. Phys.*, **67**, *2*, 483 (2015).

21. Reference Input Parameter Library IAEA-RIPL3, Segment 1, "Nuclear Masses and Deformations," Database of Audi and Wapstra, International Atomic Energy Agency Nuclear Data Services.

22. O. A. BATENKOV et al., *AIP Conf. Proc.*, **769**, 1003 (2005).

23. C. TSUCHIYA et al., *J. Nucl. Sci. Technol.*, **37**, *11*, 941 (2000); https://doi.org/10.1080/18811248.2000.9714976.

24. K. NISHIO et al., *Nucl. Sci. Technol.*, **32**, *5*, 404 (1995); https://doi.org/10.1080/18811248.1995.9731725.

25. V. F. APALIN et al., *J. Nucl. Phys.*, **71**, *3*, 553 (1965); https://doi.org/10.1016/0029-5582(65)90765-0.

26. J. S. FRASER and J. C. D. MILTON, "Nuclear Fission," *Ann. Rev. Nucl. Sci.*, **16**, 379 (1966); https://doi.org/10.1146/annurev.ns.16.120166.002115.

27. EXFOR Experimental Nuclear Data Library, Target Pu-239, Reaction (n,f), Quantity MFQ, Entries 41502006, 22650004, 23012008, 41397002, 14369002, International Atomic Energy Agency Nuclear Data Services; https://www-nds.iaea.org (current as of Feb. 8, 2018).

28. A. C. WAHL, *Atom. Data Nucl. Data Tables*, **39**, 1 (1988); https://doi.org/10.1016/0092-640X(88)90016-2.

29. R. MULLER et al., KfK 3220, Kernforschungszentrum Karlsruhe, file:///C:/Users/Owner/Downloads/KFK3220.pdf (1981) (current as of Feb. 8, 2018).

30. K. NISHIO et al., *Nucl. Phys. A*, **632**, 540 (1998); https://doi.org/10.1016/S0375-9474(98)00008-6.

31. J. W. BOLDEMAN, A. R. D. L. MUSGROVE, and R. L. WALSH, *Aust. J. Phys.*, **24**, 821 (1971); https://doi.org/10.1071/PH710821.

32. A. S. VOROBYEV et al., *EPJ Web of Conf.*, **8**, 03004 (2010); https://doi.org/10.1051/epjconf/20100803004.

33. E. E. MASLIN, A. L. RODGERS, and W. G. F. CORE, "Prompt Neutron Emission from U-235 Fission Fragments," *Phys. Rev.*, **164**, 1520 (1971).

34. A. GÖÖK, F.-J. HAMBSCH, and S. OBERSTEDT, *EPJ Web of Conf.*, **169**, 00004 (2018); https://doi.org/10.1051/epjconf/201816900004.

35. R. MUELLER et al., *Phys. Rev. C*, **29**, 885 (1984); https://doi.org/10.1103/PhysRevC.29.885.

36. EXFOR Experimental Nuclear Data Library, Target U-235, Reaction (n,f), Quantity MFQ, Entries 14369003, 22464005, 30909006, 41516018, 21095002-21095005, 21834009, 21834010, International Atomic Energy Agency Nuclear Data Services; https://www-nds.iaea.org (current as of Feb. 8, 2018).

37. N. I. AKIMOV, *Yad. Fiz.*, **13**, *3*, 484 (1971).

38. EXFOR Experimental Nuclear Data Library, Targets Pu-239, Reaction (n,f), Quantity FY (Entry 40144), International Atomic Energy Agency Nuclear Data Services; https://www-nds.iaea.org (current as of Feb. 8, 2018).

39. C. S. STRAEDE, C. BUDTZ-JORGENSEN, and H. H. KNITTER, *Nucl. Phys. A*, **462**, 85 (1987); https://doi.org/10.1016/0375-9474(87)90381-2.

40. A. AL-ADILI et al., *Phys. Rev. C*, **86**, *5*, 054601 (2012); https://doi.org/10.1103/PhysRevC.86.054601.

41. EXFOR Experimental Nuclear Data Library, Target U-235, Reaction (n,f), Quantity MFQ, PR NU, Entries 10574003, 12870004, 21785003, 20506002, 41378002, 41110006, 21252005, 20025002, 12326004, 40785002, 40388006, 40392003, 21696004, International Atomic Energy Agency Nuclear Data Services; https://www-nds.iaea.org (current as of Feb. 8, 2018).

42. EXFOR Experimental Nuclear Data Library, Target Pu-239, Reaction (n,f), Quantity MFQ, PR NU, Entries 40130004, V0018002, V0015008, 10162002, 20490003, 30006004, 20568004, 40429004, 40148003, 40033003, 20052002, 40058003, 40388007, 12326006, 40265002, 20503002, 21135007, 21139004, 14297009, 12337004, 40639002, 12833011, 21484003, V0010005, 12395003, 12357004, 21696006, 30772004, V0045004, 40871002, International Atomic Energy Agency Nuclear Data Services; https://www-nds.iaea.org (current as of Feb. 8, 2018).

43. R. E. HOWE and T. W. PHILLIPS, BNL-NCS 21501, p. 66, Brookhaven National Laboratory (1976).

44. R. E. HOWE, *Nucl. Sci. Eng.*, **86**, 157 (1984); https://doi.org/10.13182/NSE84-A18198.

45. J. FRÉHAUT, Personal Communication, CEA-DAM Bruyères-le-Châtel, France (2002).

46. J. FRÉHAUT, *Proc. Int. Conf. Nuclear Data for Science and Technology (ND1982)*, Antwerpen, Belgium, 1982, p. 78 (1982).

47. T. ETHVIGNOT et al., *Phys. Rev. Lett.*, **94**, 052701 (2005); https://doi.org/10.1103/PhysRevLett.94.107601.

48. Y. A. KHOKHLOV et al., *Proc. Int. Conf. Nuclear Data for Science and Technology (ND-1994)*, Gatlinburg, Tennessee, May 9–13, 1994, Vol. 1, p. 272, American Nuclear Society (1994).

49. G. S. BOIKOV et al., *J. Yad. Fiz.*, **53**, *3*, 628 (1991).

50. P. FIELDHOUSE et al., *J. Nucl. Energy A/B*, **20**, 549 (1966); https://doi.org/10.1016/0368-3230(66)90052-8.

51. H. CONDE, *J. Arkiv Für Fysik*, **29**, 293 (1965).

52. J. C. HOPKINS and B. C. DIVEN, *Nucl. Phys.*, **48**, 433 (1963); https://doi.org/10.1016/0029-5582(63)90182-2.

53. J. A. VASIL'EV et al., *J. Exptl. Theoret. Phys.*, **38**, *3*, 671 (1960).

54. G. N. SMIRENKIN et al., *J. Sov. At. Energy*, **4**, *2*, 253 (1958); https://doi.org/10.1007/BF02207352.

55. A. N. PROTOPOPOV and M. V. BLINOV, *J. Atomnaya Energiya*, **4**, *2*, 374 (1958).

56. I. JOHNSTONE, AERE-NP/R-1912, United Kingdom Atomic Energy Research Establishment at Harwell (1956).

57. J. W. BOLDEMAN and R. L. WALSH, *J. Nucl. Energy*, **24**, *4*, 191 (1970); https://doi.org/10.1016/0022-3107(70)90035-3.

58. N. P. KOLOSOV et al., *J. Atomnaya Energiya*, **32**, *1*, 83 (1972).

59. L. ZU-HUA, Report No. 75007, China Institute of Atomic Energy, Beijing (1976).

60. F. MANERO and V. A. KONSHIN, *Atomic Energy Review*, **10**, 637 (1972).

61. L. W. WESTON and J. H. TODD, *Phys. Rev. C*, **10**, 1402 (1974); https://doi.org/10.1103/PhysRevC.10.1402.

62. M. SOLEILHAC, J. FRÉHAUT, and J. GAURIAU, *J. Nucl. Energy*, **23**, 257 (1969); https://doi.org/10.1016/0022-3107(69)90060-4.

63. R. L. WALSH and J. W. BOLDEMAN, *J. Nucl. Energy*, **25**, 321 (1971); https://doi.org/10.1016/0022-3107(71)90064-5.

64. M. SOLEILHAC et al., *Proc. Int. Conf. Nuclear Data for Reactors*, Helsinki, Finland, 1970, Vol. 2, p. 145, International Atomic Energy Agency (1970).

65. B. NURPEISOV et al., *J. Atomnaya Energiya*, **39**, *3*, 199 (1975).

66. K. E. VOLODIN et al., *J. Atomnaya Energiya*, **33**, *5*, 901 (1972).

67. V. G. NESTEROV et al., *Proc. Int. Conf. Nuclear Data for Reactors*, Helsinki, Finland, 1970, Vol. 2, p. 167, International Atomic Energy Agency (1970).

68. H. CONDE, J. HANSEN, and M. HOLMBERG, *J. Nucl. Energy*, **22**, 53 (1968); https://doi.org/10.1016/0022-3107(68)90064-6.

69. M. V. SAVIN et al., *Proc. Int. Conf. Nuclear Data for Reactors*, Helsinki, Finland, 1970, Vol. 2, p. 157, International Atomic Energy Agency (1970).

70. G. N. SMIRENKIN et al., *Atomnaya Energiya*, **4**, *2*, 188 (1958).

71. V. P. ZOLOTSKIJ et al., *Proc. Conf. Neutron Physics*, Kiev, Soviet Union, 1973, Vol. 4, p. 70 (1973).

72. Y. RYABOV et al., *Nucl. Phys. A*, **216**, 395 (1973); https://doi.org/10.1016/0375-9474(73)90475-2.

73. D. S. MATHER, P. FIELDHOUSE, and A. MOAT, *J. Nucl. Phys.*, **66**, 149 (1965); https://doi.org/10.1016/0029-5582(65)90139-2.

74. B. C. DIVEN et al., *Phys. Rev.*, **101**, 1012 (1956); https://doi.org/10.1103/PhysRev.101.1012.

75. E. BARNARD et al., *Nucl.Phys.*, **71**, 228 (1965); https://doi.org/10.1016/0029-5582(65)90048-9.

76. B. C. DIVEN and J. C. HOPKINS, *Proc. Physics of Fast and Intermediate Reactors Seminar*, Vienna, Austria, August 3–11, 1961, Vol. 1, p. 149, International Atomic Energy Agency (1961).

77. N. N. FLEROV and V. M. TALYZIN, *Atomnaya Energiya*, **10**, 68 (1961).

78. R. GWIN, R. R. SPENCER, and R. W. INGLE, *Nucl. Sci. Eng.*, **87**, 381 (1984); https://doi.org/10.13182/NSE84-A18506.

79. M. JACOB, Report No. 652, p. 23, Centre d`Etudes Nucléaires (1958).

80. J. W. BOLDEMAN, *Proc. Int. Specialists Symp. Neutron Standards and Applications*, Gaithersburg, Maryland, March 28–31, 1977, p. 182, National Bureau of Standards (1977).

81. T. SNYDER and R. WILLIAMS, Report No. 102, Los Alamos Scientific Laboratory (1944).

82. D. E. McMILLAN et al., Report No.1464, Knolls Atomic Power Laboratory (1955).

83. J. W. BOLDEMAN and M. G. HINES, *Nucl. Sci. Eng.*, **91**, 114 (1985); https://doi.org/10.13182/NSE85-A17133.

84. N. E. HOLDEN and M. S. ZUCKER, *Nucl. Sci. Eng.*, **98**, 174 (1988); https://doi.org/10.13182/NSE88-A28498.

85. V. N. NEFEDOV, B. I. STAROSTOV, and A. A. BOITSOV, *Proc. All-Union Conf. Neutron Physics*, Kiev, Soviet Union, October 2–6, 1983, Vol. 2, p. 285 (1983).

86. JENDL4 Evaluated Nuclear Data Library, ZA=092235 and 094239, MF=3, MT=18, 19, 20, 21, 38, International Atomic Energy Agency Nuclear Data Services; https://www-nds.iaea.org (current as of Feb. 8, 2018).

87. G. VLADUCA et al., *Nucl. Phys. A*, **740**, 3 (2004); https://doi.org/10.1016/j.nuclphysa.2004.04.113.

88. G. VLADUCA et al., *Nucl. Phys. A*, **767**, 112 (2006); https://doi.org/10.1016/j.nuclphysa.2005.12.017.

89. E. RICH et al., *Nucl. Sci. Eng.*, **162**, 178 (2009); https://doi.org/10.13182/NSE162-178.

90. A. TUDORA, F.-J. HAMBSCH, and S. OBERSTEDT, *Nucl. Phys. A*, **917**, 43 (2013); https://doi.org/10.1016/j.nuclphysa.2013.09.002.

91. ENDF/B-VIII Evaluated Nuclear Data Library, File ZA094239: MF=1, MT=456 (Average Number of Prompt

Neutrons per Fission), International Atomic Energy Agency Nuclear Data Services; https://www-nds.iaea.org (current as of Feb. 8, 2018).

92. JENDL4 Evaluated Nuclear Data Library, File ZA094239: MF=1, MT=456 (Average Number of Prompt Neutrons per Fission), International Atomic Energy Agency Nuclear Data Services; https://www-nds.iaea.org (current as of Feb. 8, 2018).

93. JEFF3.3 Evaluated Nuclear Data Library, File ZA094239: MF=1, MT=456 (Average Number of Prompt Neutrons per Fission), International Atomic Energy Agency Nuclear Data Services; https://www-nds.iaea.org (current as of Feb. 8, 2018).